Gum Acacia as a Facile Reducing, Stabilizing, and Templating Agent for Palladium Nanoparticles

D. Keerthi Devi, S. Veera Pratap, R. Haritha, K. Samba Sivudu, P. Radhika, B. Sreedhar

Inorganic and Physical Chemistry Division, Indian Institute of Chemical Technology, Council of Scientific and Industrial Research, Hyderabad 500 607, India

Received 1 September 2009; accepted 20 June 2010
DOI 10.1002/app.33004
Published online 8 March 2011 in Wiley Online Library (wileyonlinelibrary.com).

ABSTRACT: This article presents the findings of a facile and effective nanoparticle synthesis approach based on aqueous solutions of gum acacia (GA), also known as gum arabic without the addition of any toxic reagents either for the reduction or capping for the effective stabilization of palladium (Pd) nanoparticles with a narrow size distribution (with a H_2PdCl_4/GA ratio of 1:29.411, the solution the average diameter was 9.1 nm, and the standard deviation was ±0.3 nm). In this approach, the particle size was controlled by the manipulation of the temperature, time, and concentration of GA. The synthesized Pd nanoparticles were well characterized by ultraviolet–visible spectroscopy, Fourier transform infrared spectroscopy, X-ray diffraction, transmission electron microscopy, X-ray photoelectron spectroscopy, dynamic light scattering, and thermogravimetric analysis. This route was very simple and reproducible, and further study on the application of these nanoparticles for various organic transformations is underway. © 2011 Wiley Periodicals, Inc. J Appl Polym Sci 121: 1765–1773, 2011

Key words: palladium; bio-compatibility; biomaterials; biopolymers; colloids

INTRODUCTION

Over the last decade, the meticulous understanding of science at the nanometer scale has attracted the interest of numerous groups all over the world and has led to the emergence of a new interdisciplinary field called *nanoscience* because of the size-dependent optical, electronic, and catalytic properties of nanoparticles.[1] The physical and chemical properties are enormously different, both quantitatively and qualitatively, from those of bulk materials as these materials are derived by manipulation at the atomic or molecular levels.[2,3] The development of reliable synthetic methodologies for the synthesis of nanoparticles with a narrow size distribution and for the control of the assembly of these well-defined nanoparticles has always been critically important for fundamental scientific and technological applications.[4] To produce monodisperse nanoparticles as building blocks for the assembly of an ordered architecture, capping agents have been used to effectively passivate the surfaces and suppress the growth of particles through strong interactions with the particles via their functional molecular groups[5,6] and drug delivery.[7] The controlled fabrication of nanometer-scale objects is without a doubt one of the central issues in current science and technology.[8]

Of the various strategies used, chemical reduction has proved to be an ideal strategy for the generation of uniform nanoparticles with a narrow size distribution via microemulsion,[9] coprecipitation,[10] carbon nanotube,[11] and polymer protection methods.[12–14] Biological macromolecules,[15,16] block copolymers,[17,18] dendrimers,[19,20] liquid crystals,[21] latex particles,[22] mesoporous inorganic materials,[5,23] microgels,[24] and hydrogels[25,26] have been used as templates for the production of well-dispersed nanoparticles. Metal nanoparticles have been extensively studied for many years because they usually exhibit unique properties and can be potentially used in many applications, including optics,[1] catalysis,[2] biodiagnostics,[3] and surface-enhanced Raman scattering.[27,28] The chemical and physical properties of metal nanoparticles depend not only on their size but also on their morphology. Many successful attempts to prepare nanoparticles of Pt group metals have been reported; so far, they have a characteristically high surface-to-volume ratio, and in particular, palladium (Pd) nanoparticles have been used as catalysts for many organic transformations. Nath et al.[29] reported the synthesis of Pd nanoparticles from an aqueous Pd(II) chloride solution in polyoxyethylene isooctyl phenyl ether (Triton X-100, TX-100) under UV irradiation. Water-soluble Pd nanoparticles have also been stabilized by thiolated β-cyclodextrin[30] and isocyanide ligands.[31] El-Sayed and coworkers[32,33] described the synthesis and catalytic activity of Pd

Correspondence to: B. Sreedhar (sreedharb@iict.res.in).

nanoparticles prepared in the presence of different stabilizers, such as polyamidoamino dendrimers[32] and block copolymers.[33] The synthesis of these stabilizers was very difficult and also not environmentally friendly. To overcome this problem, many researchers have used natural polymers, such as chitosan[34–36] and arabinogalactan.[37] As is the common practice, in the previous study, they also used $NaBH_4$ or hydrazine hydrate to reduce the metal precursors. Most of these methods have an impact on the greenhouse effect. Therefore, to overcome all of these problems, various groups have adopted green chemistry principles over the last 5 years to develop environmentally friendly methods. For example, silver and gold nanoparticles produced from vegetable oil are being used in antibacterial paints.[38] Now, many researchers have identified environmentally friendly materials that are multifunctional. With all this in mind, researchers are selecting naturally available compounds, such as coffee and tea leaves,[39] sugarcane extracts,[40] and gum acacia (GA), also known as gum arabic.[41] Generally, GA, is a highly branched, neutral or slightly acidic arabinogalactan polysaccharide obtained naturally from the stems and branches of the *Acacia senegal* tree. The nontoxic and biocompatible properties of GA have made it widely used in the food and pharmaceutical industries as additives or emulsifying agents. Moreover, it has also been increasingly used as a stabilizer for various novel nanomaterials, such as carbon nanotubes,[42] nanogold,[43] nanosilver,[44] and oxide nanoparticles.[45,46] GA also shows a superb dispersing ability in the preparation of quantum dot nanocolloids.[47] In our previous study,[48] we used naturally occurring GA for the reduction and stabilization of silver nanoparticles at room temperature. In an attempt to further continue research in this area, we herein describe a straightforward approach for the aqueous-phase synthesis of Pd nanoparticles with GA as a reducing and stabilizing agent. The effects of the manipulation of the temperature, pH, time, and concentration of GA were studied in detail.

EXPERIMENTAL

Materials

All of the chemicals we used (GA, HCl, and NaOH) were analytical grade. GA (spray-dried Laboratory Reagent (LR)) was purchased from S. D. Fine Chemical (Mumbai, India), and the precursor Pd(II) chloride (reagent plus, 99%) was obtained from Sigma Aldrich Chemical Co., Inc. (Seelze, Germany). All aqueous solutions were prepared with deionized water from a Milli Q water system Billerica, MA, USA (18.2 MΩ cm).

Synthesis of the Pd nanoparticles

Accurately, $PdCl_2$ (0.106 g) was dissolved in 300 mL of 8×10^{-4} *M* HCl to form a H_2PdCl_4 aqueous solution; this was used as a stock solution. An aliquot of 5 mL of the aqueous H_2PdCl_4 solution was mixed with 5 mL of a 0.2% aqueous solution of acacia. The reaction mixture was heated at different temperatures (40, 60, 80, and 100°C) for 6 h. Within several minutes, the color of the solution changed from light yellow to a deep brown; this indicated the formation of nanoparticles. The progress of the Pd reduction was monitored spectrophotometrically at regular intervals from 60 to 360 min. The addition of acetone followed by centrifugation isolated the Pd nanoparticles in the form of a dark brown powder. The resulting powder was readily redispersible in water, which afforded a transparent brown suspension of well-dispersed nanoparticles. Similar experiments were carried out for 5 mL of 0.2, 0.4, 0.6, 0.8, and 1% aqueous GA solutions.

Characterization

The synthesized Pd nanoparticles were well characterized us with ultraviolet–visible (UV–vis) spectroscopy, transmission electron microscopy (TEM), X-ray diffraction (XRD), X-ray photoelectron spectroscopy (XPS), Fourier transform infrared (FTIR) spectroscopy, dynamic light scattering (DLS), and thermogravimetric analysis (TGA). TEM samples were prepared by the placement of the sample mixture drops directly on Formvar polymer-coated grids with a micropipette. The Pd nanoparticles present in the aqueous mixture were allowed to settle, and the extra solvent was subsequently removed by placement of the TEM grid on neat filter paper and drying at ambient temperature for half a day. The morphology, size, and shape distribution of the Pd nanoparticles were recorded with a TECNAI FE12 TEM (Eindhonen, The Netherlands) instrument operating at 120 kV. In each image, more than 150 particles were analyzed with SIS imaging software to create size distribution histograms (Munster, Germany). The diffraction patterns were recorded at selected areas to determine the crystal structure and phases of the crystals at a 660-mm camera length.

All UV–vis spectrophotometric characterization of the Pd GA aqueous dispersions were carried out on a Cintra 10^e spectrophotometer (Braeside, Australia) with quartz cuvette cells with a 1-cm path length. The colloid samples were usually diluted with water by a factor of 5 or more if necessary and examined over the 900–190 nm region with a scan rate of 60 nm/min. XRD measurements of the Pd nanoparticles were recorded with a Rikagu diffractometer (Tokyo, Japan, Cu radiation, $\lambda = 0.1546$ nm) running at 40 kV and 40

mA. IR spectra of the acacia and acacia–Pd nanoparticles were recorded with a Thermo Nicolet Nexus 670 spectrophotometer (Washington, United States). The particle size was determined by DLS measurements. These experiments were carried in Zetasizer Nano ZS (Malvern) instrument (Worcestershire, UK) by dispersion of the nanoparticles in water. The run time of the measurements was 70 s. The particle size distribution curve was obtained by the average of 10 measurements. TGA was carried out on a TGA/SDTA Mettler Toledo 851^e system (Zurich, Switzerland) with open alumina crucibles containing samples weighing about 8–10 mg with a linear heating rate of 10°C/min. Nitrogen was used as purge gas for all of these measurements. XPS measurements were obtained on a KRATOS-AXIS 165 instrument equipped with dual aluminum–magnesium anodes with Mg Kα radiation (1253.6 eV) operated at 5 kV and 15 mA with a pass energy of 80 eV and an increment of 0.1 eV. The samples were degassed out for several hours in an XPS chamber to minimize air contamination to the sample surface. To overcome the charging problem, a charge neutralizer of 2 eV was applied, and the binding energy (BE) of the C1s core level (BE = 284.6 eV) of adventitious hydrocarbon was used as a standard. The XPS spectra were fitted with a nonlinear square method with the convolution of Lorentzian and Gaussian functions after a polynomial background was subtracted from the raw spectra.

RESULTS AND DISCUSSION

In early days of colloid science, plant extracts and gums were used routinely to stabilize colloidal metal dispersions.[49] In that category, GA is a well known polysaccharide with a high molecular weight that can be derived from the acacia tree. GA is a water-soluble polysaccharide obtained from the gummy exudates of the acacia tree. GA consists of three main fractions:

1. The major one is a highly branched polysaccharide consisting of a β-(1-3)-galactose backbone with linked branches of arabinose and rhamnose, which terminate in glucuronic acid.
2. A smaller fraction (~ 10 wt % of the total) is an arabinogalactan–protein complex [GAGP (gum acaia-glycoprotein)], in which arabinogalactan chains are covalently linked to a protein chain through serine and hydroxyproline groups. The attached arabinogalactan in the complex contains about 13 mol % glucoronic acid.
3. The smallest fraction (~ 1% of the total), with the highest protein content (~ 50 wt %), is a glycoprotein that differs in its amino acids composition from that of the GAGP complex. Here, the functional group (—OH) present in arabinose and rhamnose and —COOH of gluconic acids play a crucial role in the formation metal nanoparticles, whereas the proteinaceous core with amino acids stabilizes the formed metal nanoparticles.

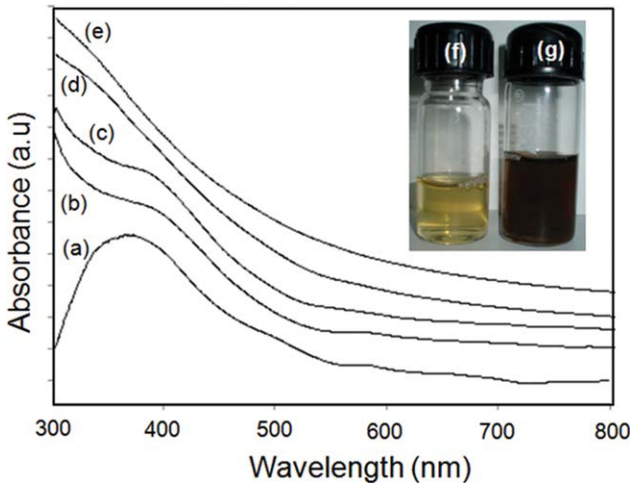

Figure 1 UV–vis spectra of acacia to Pd ratio of 1:29.411 at different temperatures: (a) room temperature and (b) 40, (c) 60, (d) 80, and (e) 100°C for 6 h. The inset shows photographs of the reaction mixture at (f) 0 min and (g) after heating at 100°C for 6 h. [Color figure can be viewed in the online issue, which is available at wileyonlinelibrary.com.]

UV analysis

Recent studies have focused on the synthesis of metal nanoparticles with polymeric templates in the absence of typical chemical reducing agents.[50–55] In addition to the established strategies, in this study, we used a simple and highly facile template-based methodology to prepare Pd nanoparticles with GA polymer without the addition of any reducing agent. In this study, when a mixture of H_2PdCl_4 and acacia was kept overnight at room temperature, no color change was observed; this clearly indicated that there no sign of reduction of the Pd(II) ions. This speaks for the essentiality of heating the reaction mixture at higher temperatures for the reduction of Pd(II). Previously, either UV irradiation or heating helped to produce Pd particles in H_2O, 2-propanol, glycerol, and poly(vinyl alcohol) media.[29] Marked changes were observed in the surface plasmon peak at 400 nm when the reaction mixtures were heated at different temperatures (40, 60, 80, and 100°C), as shown in Figure 1. The optimized reaction temperature was found to be 100°C, as there was no surface plasmon band in the range 200–800 nm; this indicated that most of the Pd(II) was reduced to the Pd(0) state.

FTIR and TGA studies

Stabilization of the Pd nanoparticles via the functional groups of acacia (namely, —COOH and —OH)

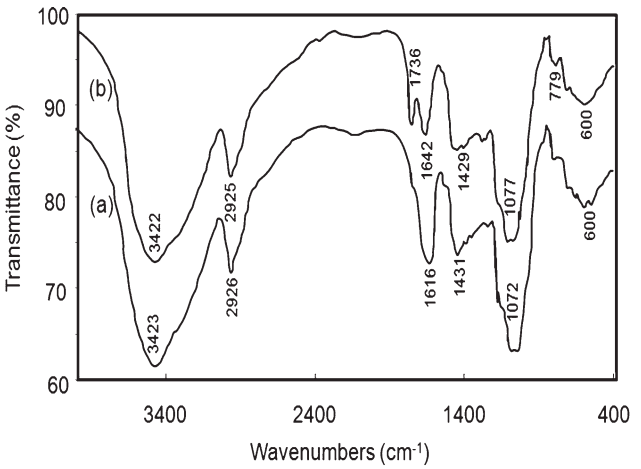

Figure 2 FTIR spectra of the (a) pure acacia and (b) acacia–Pd nanoparticles.

was examined by the comparison of the FTIR spectrum of neat acacia gum and the FTIR spectrum of the acacia-capped Pd nanoparticles (Fig. 2). A solid sample for FTIR analysis was prepared with the acacia-capped Pd nanoparticles, which were recovered from the aqueous solution via centrifugation with acetone as an antisolvent. When the acacia molecule anchored to the nanoparticle surfaces, the stretching frequencies originating from the functional groups of acacia were expected to shift accordingly. The stretching vibration of —OH at 3423 cm^{-1} shifted to 3422 cm^{-1}, and the asymmetric and symmetric stretching vibrations of $—CH_2$ at 2926 and 2850 cm^{-1} shifted to 2923 and 2845 cm^{-1}, respectively. The peaks at 1616 cm^{-1} (C=O stretching of the carbonyl group, typical saccharide absorption) and 1431 cm^{-1} (C=O stretching of the —COOH group and —OH bending of the acid group, respectively) showed a shift to 1642 and 1429 cm^{-1}, respectively. The extra shoulder peak observed at 1736 cm^{-1} indicated the attachment of COO^- to the surface of the Pd nanoparticles. The interaction between the acacia and Pd nanoparticles via both the —COO and —OH functional groups facilitated the encapsulation of Pd nanoparticles with a protective layer of acacia molecules; this provided steric stabilization of the Pd nanoparticles. Considering the steric structure of acacia, it was reasonable to assume that only some of the —COO and —OH groups in acacia molecules interacted with the particles. As such, the remaining negatively charged —COO groups underwent electrostatic repulsion with other particles and the amino acid proteinaceous core, which provided further stabilization for the Pd nanoparticles. Accordingly, the green and inexpensive naturally occurring acacia gum not only worked as a reducing agent but also passivated the surface of the Pd nanoparticles (via covalent chemical interactions) and suppressed the growth and agglomeration of the particles (via both electrostatic repulsion and steric hindrance) in the system. In comparison with β-D-glucose, which stabilizes particles via its hydroxyl groups, the additional interaction imposed by the —COOH groups of the acacia molecules with the Pd nanoparticles played an important role in narrowing the particle size distribution; this was clearly shown in the TEM images. The biocompatibility of the acacia gum protected the metal nanoparticles, so they could be more readily integrated into systems relevant for pharmaceutical, biomedical, and biosensor applications.

To determine the influence of temperature on GA, IR spectra were recorded for acacia samples annealed at various temperatures (40, 60, 80, and 100°C). As shown in Figure 3, the IR spectra for samples annealed at different temperatures did not show any changes in the observed IR peaks; this clearly suggested that the optimum temperature of 100°C used in this study had no influence on the degradation of the polymer. In addition, TGA thermograms were recorded for the pure acacia and acacia–Pd nanoparticles (Fig. 4). As shown in Figure 4, the initial thermal stability of pure acacia was about 260°C; this also suggested that the optimum temperature used in this study did not contribute to any

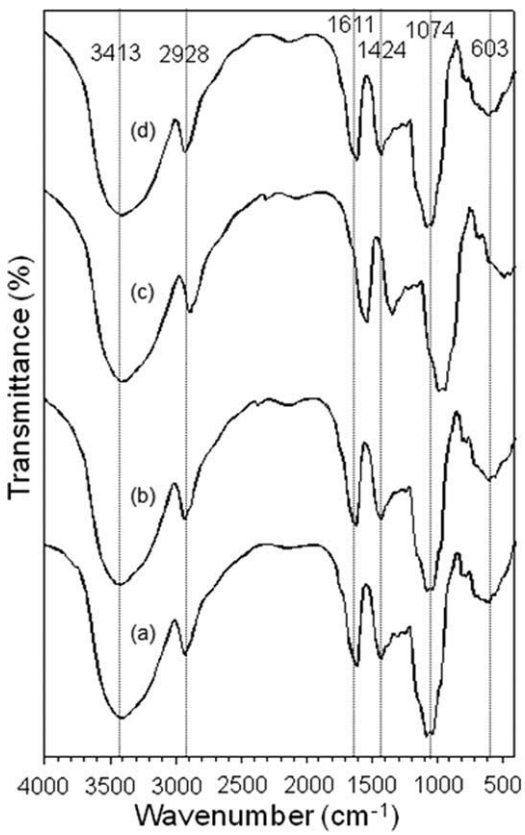

Figure 3 FTIR spectra of the pure acacia annealed at different temperatures: (a) 100, (b) 80, (c) 60, and (d) 40°C.

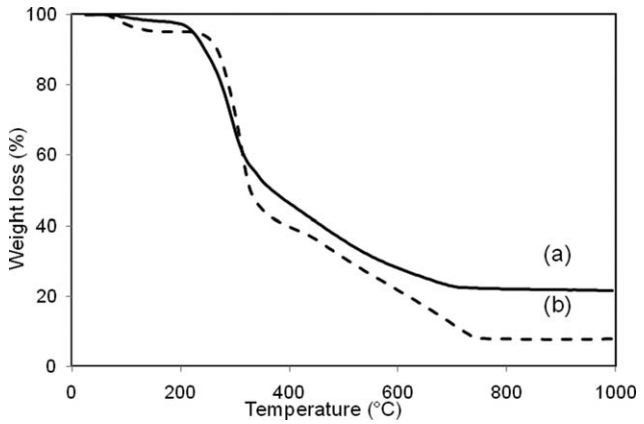

Figure 4 TGA thermograms of the (a) pure acacia and (b) acacia–Pd nanoparticles.

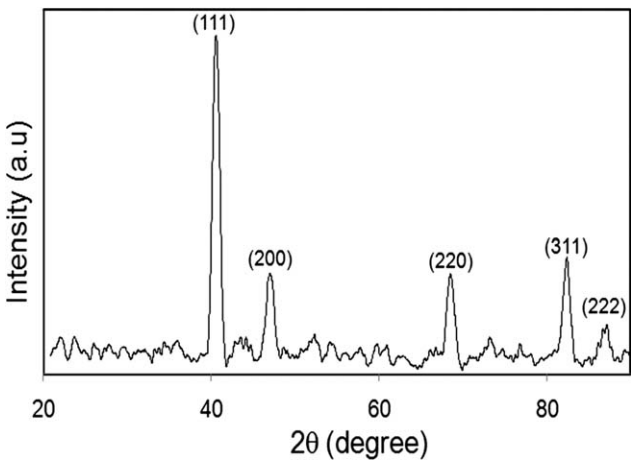

Figure 5 Powder XRD pattern of the acacia–Pd nanoparticles prepared with the Pd precursor and acacia gum at 100°C at a ratio of 1 : 29.411.

degradation of the polymer during the synthesis of the acacia-stabilized Pd nanoparticles.

XRD analysis

Figure 5 shows the XRD pattern of the acacia-stabilized Pd nanoparticles synthesized at 100°C. All of the peaks were clearly distinguished. The broad peak at 40.2° was characteristic of the (111) peak of zero-valent Pd with a face-centered cubic structure. The other four diffraction peaks with 2θ values of 46.7, 68.0, 81.9, and 86.7° corresponded to the major reflections of the (200), (220), (311) and (222) crystal planes, respectively.[56,57] The nanoparticle size was also calculated from the line broadening of the (111) reflection with the Debye–Scherrer equation. The average diameter of the Pd nanoparticles was calculated as 9.5 nm; this was in consonance with the size of the nanoparticles observed with TEM.

TEM micrographs

The modulation of the reaction condition played a significant role in the control of the size and shape of the particles. We investigated the effects of the (1)

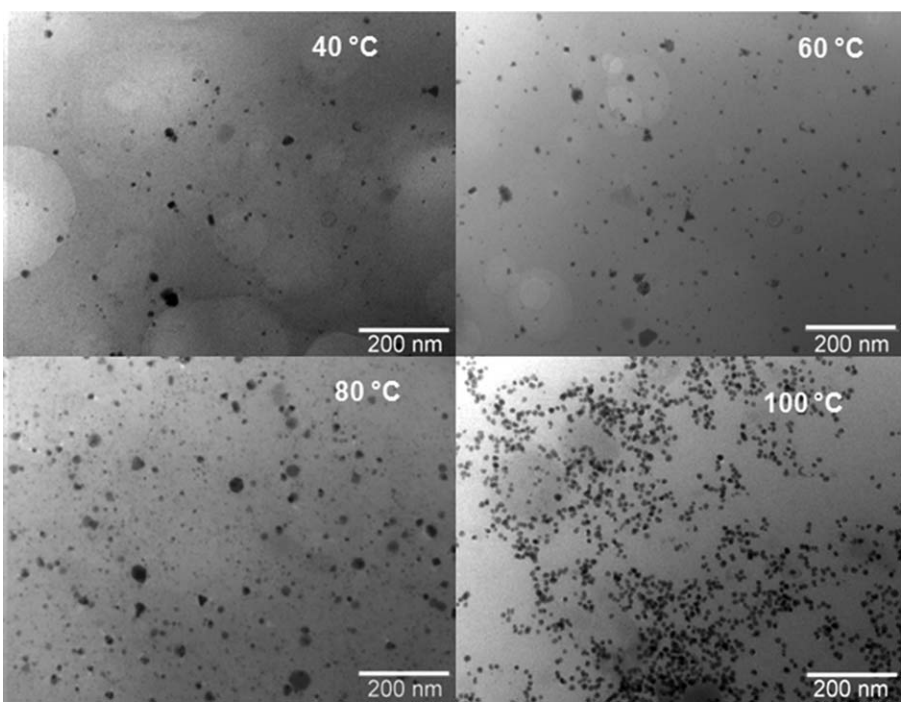

Figure 6 TEM images of the Pd nanoparticles prepared with the Pd precursor and acacia gum at the ratio of 1 : 29.411 prepared at different temperatures.

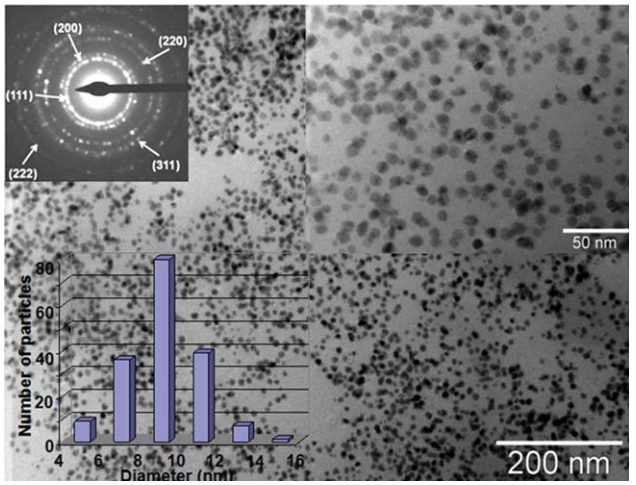

Figure 7 TEM image of the Pd nanoparticles prepared with the Pd precursor and acacia gum at 100°C at a ratio of 1:29.411. The insets show the typical selected area electron diffraction pattern, a TEM image at higher magnification, and a histogram showing the particle size distribution of the Pd nanoparticles. [Color figure can be viewed in the online issue, which is available at wileyonlinelibrary.com.]

reaction temperature and (2) concentration of acacia. Figure 6 shows the TEM images of the Pd nanoparticles synthesized with GA as a reducing agent at different temperatures. As shown, an increase in the reaction temperature resulted in an increase in the population of Pd nanoparticles, which was accompanied by a narrower size distribution. At 100°C (Fig. 7), we observed that the Pd nanoparticles were uniform in size with a spherical shape, and the histogram, shown as an inset in Figure 7, clearly showed that the average diameter of the particles was 9.0 nm. The selected area electron diffraction pattern, shown as inset in Figure 7, exhibited five main diffused rings that were characteristic of the kinds of crystalline orientation and were indexed to be the (111), (200), (220), (311), and (222) reflections of the face-centered cubic Pd.

To study the influence of the acacia concentration on the synthesis of the Pd nanoparticles, reactions were conducted with different ratios of Pd precursor to acacia (1:5.88, 1:11.76, 1:17.64, and 1:23.52). The size of the Pd nanoparticles decreased with increasing acacia concentration from 20.0 to 15.15 to 9.88 to 9.6 nm, respectively. The gradual variation in the size of the nanoparticles was revealed clearly in the TEM pictures (Fig. 8). The hyperbolic nature of the curve obtained from the plot of the size of the Pd nanoparticles against the acacia concentration (Fig. 9) implied that size of the nanoparticles decreased gradually with increasing acacia concentration, and a limiting value was reached as the surface of the particles was saturated with the capping agent. The diameter determined by DLS measurements was strongly influenced by larger particles because of increasing scattering with increasing particles size. However, in consideration of the differences of the characterization methods and difficulties caused by a broad size distribution, the observed results were

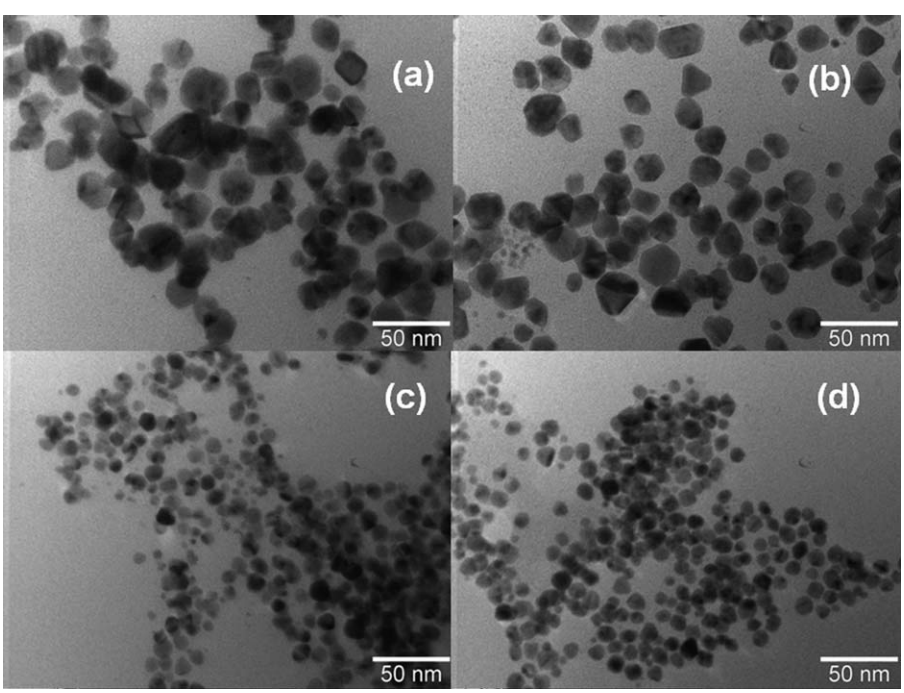

Figure 8 TEM images of the Pd nanoparticles prepared with the Pd precursor and acacia gum at ratios of (a) 1 : 5.88, (b) 1 : 11.76, (c) 1 : 23.52, and (d) 1 : 29.411.

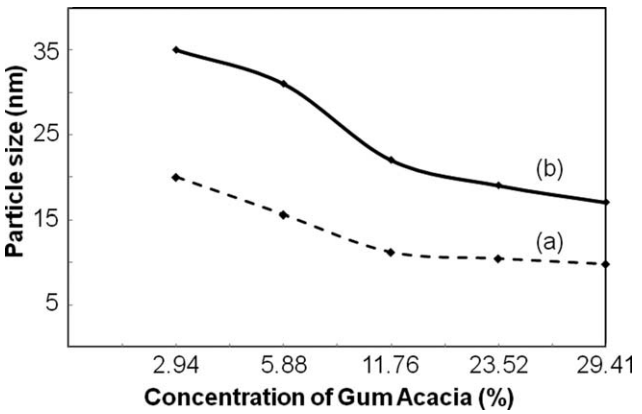

Figure 9 Influence of the GA concentration on the particle size distribution of the acacia–Pd nanoparticles with (a) TEM and (b) DLS.

in good agreement and showed similar trends as observed by TEM. The monodispersed nanoparticles, as shown in the TEM images at higher concentrations (Fig. 10), that is, above 29.411, were attributed to the effective passivation of the surfaces and suppression of the growth of the nanoparticles through strong interactions with the particles via the functional molecular groups of acacia, namely, the hydroxyl groups of arabinose and rhamnose galactose and the carboxylic groups of glucoronic acid moieties. Acacia has been shown to be an effective capping agent because of the well-established chemical bonding between the —OH and —COOH functional groups and the surface of the metallic nanoparticles; they, thereby, form a transparent colloidal suspension (Fig. 1). It was also remarkable that this colloidal solution on drying-form solid-state nanocomposite and could be reconstituted again in aqueous media without the loss of its nanoparticulate properties. The synthetic method developed here is potentially useful for the large-scale production of uniform size Pd nanoparticles with commonly available GA.

XPS studies

To determine the structural features of the GA–Pd nanoparticles, XPS studies were performed on the GA, GA–Pd nanocomposite, and Pd nanoparticles obtained by precipitation of the reaction mixture. Pure GA was first analyzed to investigate the influence on the structure of GA on the Pd ions and nanometal particles. The C1s and Pd3d core-level spectra were collected and analyzed. The core-level BE and full width at half-maximum were analyzed with particular attention to the Pd3D spin-orbit components, which were of major interest for the assessment of the GA–Pd interactions in the nanocomposite and for the investigation of its role in the Pd ion reduction process. All of the XPS spectra were calibrated in energy with the main component of the C1s signal, which was attributed to aromatic carbons, at 284.60 eV. The observed high-resolution narrow scans of C1s for both the pure GA and Pd nanoparticles are shown in Figure 11. The observed C1s peaks could be

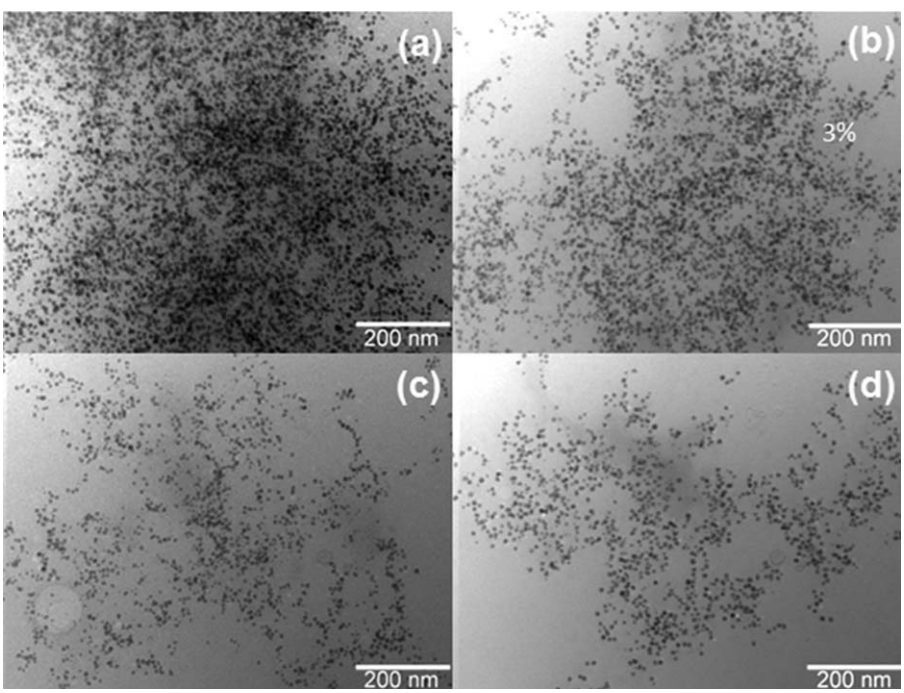

Figure 10 TEM images of the acacia–Pd nanoparticles prepared with the Pd precursor and acacia gum at 100°C at different ratios: (a) 1 : 58.82, (b) 1 : 88.23, (c) 1 : 117.64, and (d) 1 : 147.05.

deconvoluted into four peaks, and the BEs were attributed to the distinct energies for substituted carbon moieties. The observed C1s peaks at 284.6, 286.3, 287.7, and 289.2 eV were characteristic of —C—C—/—C—H—, a carbon singly bonded to one oxygen atom (—C—O—), —O—C—O—, and the carboxylic acid group (—O—C=O—), respectively. A slight shift in the BE peaks was observed for the Pd nanoparticles; this was attributed to the interaction of the functional groups of acacia with Pd metal. This was in consonance with the observation for FTIR studies. The Pd3d spectra showed the presence of a main contribution, together with a minor component at higher BE values. Curve-fitting analysis showed that the Pd3d spectra of the GA–Pd nanocomposite and Pd nanoparticles resulted from two pairs of spin-orbit components, as shown in Figure 12. On the basis of previous measurements, the Pd $3d_{5/2}$ peak found at BE = 335.5 eV was attributed to metallic palladium [Pd(0)]; this was in agreement with literature reports.[58] The second $3d_{5/2}$ signal, occurring at higher BE values (BE = 337.21 eV), was due to Pd atoms with lower charge densities. Although the presence of Pd in two oxidation states was very clear from both spectra, the higher intensity in the Pd nanoparticles clearly indicated the metallic form of the sample. The contribution due to the BE peak at about 337 eV was attributed to the presence of Pd atoms on the surface capping on the Pd nanoparticles. This also supported the presence of GA on the surface as a capping agent on the Pd nanoparticles, as observed from the FTIR spectra.

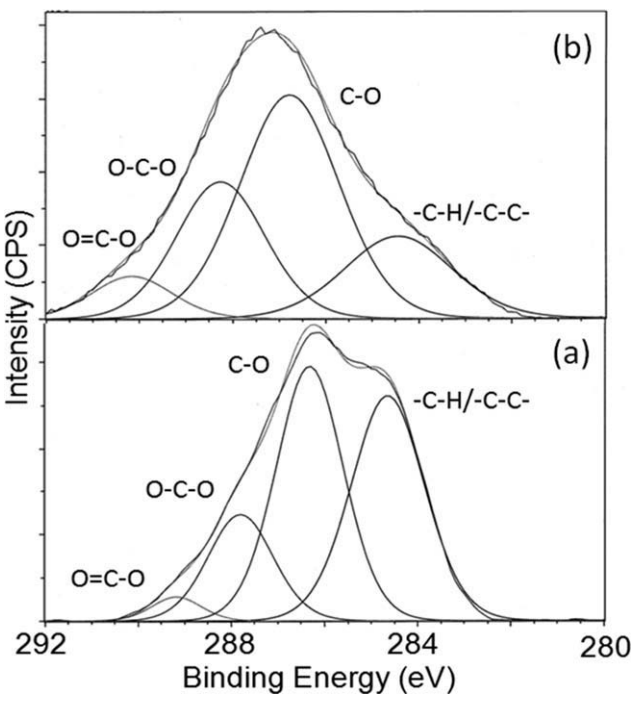

Figure 11 XPS high-resolution narrow scans of C1s for (a) GA and (b) the acacia–Pd nanoparticles.

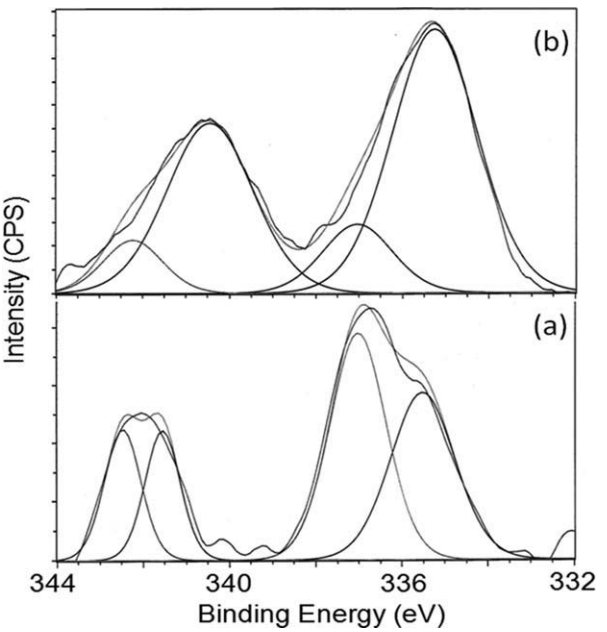

Figure 12 XPS high-resolution narrow scans of Pd 3d for the (a) acacia–Pd and (b) Pd nanoparticles.

CONCLUSIONS

In summary, a highly facile, simple, cost-effective, and green approach was developed for the synthesis of nearly monodisperse Pd nanoparticles via a simple aqueous-phase reaction between Pd^{2+} ions and naturally occurring GA. GA not only acted as a reducing agent but also worked as a stabilizer. The size and shape of the nanoparticles was easily controlled through the variation of the concentration of the acacia gum. The formation of Pd nanoparticles by the acacia polymer networks was proven with various techniques, such as FTIR, UV–vis, XRD, XPS, TGA, DLS, and TEM. The formed Pd nanoparticles were stable for 5 months. This methodology could also be adapted to the preparation of other metal nanoparticles.

References

1. Sosa, I. O.; Noguez, C.; Barrera, R. G. J Phys Chem B 2003, 107, 6269.
2. Roucoux, A.; Schulz, J.; Patin, H. Chem Rev 2002, 102, 3757.
3. Rosi, N. L.; Mirkin, C. A. Chem Rev 2005, 105, 1547.
4. Orendorff, C. J.; Gole, A.; Sau, T. K.; Murphy, C. J. Anal Chem 2005, 77, 3261.
5. Tian, Z. Q.; Ren, B. Annu Rev Phys Chem 2004, 55, 197.
6. Tian, Z. Q.; Ren, B.; Li, J. F.; Yang, Z. L. Chem Commun 2007, 34, 3514.

7. Cliffel, D. E.; Zamborini, F. P.; Gross, S. M.; Murray, R. W. Langmuir 2000, 16, 9699.
8. Ariga, K.; Hill, J. P.; Lee, M. V.; Vinu, A.; Charvet, R.; Acharya, S. Sci Technol Adv Mater 2008, 9, 014109.
9. Lisiecki, I.; Pileni, M. P. J Am Chem Soc 1993, 115, 3887.
10. Chen, D. H.; Chen, Y. Y. Mater Res Bull 2002, 37, 801.
11. Kim, D.; Lee, T.; Geckeler, K. E. Angew Chem Int Ed 2005, 45, 104.
12. Yanagihara, N.; Tanaka, Y.; Okamoto, H. Chem Lett 2001, 30, 796.
13. Gao, J.; Fu, J.; Lin, C.; Lin, J.; Han, Y.; Yu, X.; Pan, C. Langmuir 2004, 20, 9775.
14. Kuo, P. L.; Chen, W. F. J Phys Chem B 2003, 107, 11267.
15. Behrens, S.; Habicht, W.; Wagner, K.; Unger, E. Adv Mater 2006, 18, 284.
16. Naik, R. R.; Jones, S. E.; Murray, C. J.; McAulifee, J. C.; Vaia, R. A.; Stone, M. O. Adv Funct Mater 2004, 14, 25.
17. Jewrajka, S. K.; Chatterjee, U. J Polym Sci Part A: Polym Chem 2006, 44, 1841.
18. Grubbs, R. B. J Polym Sci Part A: Polym Chem 2005, 43, 4323.
19. Sun, X.; Jiang, X.; Dong, S.; Wang, E. Macromol Rapid Commun 2003, 24, 1024.
20. Okugaichi, A.; Torigoe, K.; Yoshimura, T.; Esumi, K. Colloids Surf A 2006, 273, 154.
21. Qi, L.; Gao, Y.; Ma, J. Colloids Surf A 1999, 157, 285.
22. Crooks, R. M.; Zhao, M.; Sun, L.; Chechik, V.; Yeung, L. K. Acc Chem Res 2001, 34, 181.
23. Ghosh, A.; Patra, C. R.; Mukherjee, P.; Sastry, M.; Kumar, R. Microporous Mesoporous Mater 2003, 58, 201.
24. Zhang, J.; Xu, S.; Kumacheva, E. J Am Chem Soc 2004, 126, 7908.
25. Jin, R. H.; Yuan, J. J. J Mater Chem 2005, 15, 4513.
26. Advanced Macromolecular and Supramolecular Materials and Processes; Geckeler, K. E., Ed.; Kluwer Academic/Plenum: New York, 2002.
27. Talley, C. E.; Jackson, J. B.; Oubre, C.; Grady, N. K.; Hollars, C. W.; Lane, S. M.; Huser, T. R.; Nordlander, P.; Halas, N. J. Nano Lett 2005, 5, 1569.
28. Tian, Z. Q.; Ren, B.; Annu Rev Phys Chem 2004, 55, 197.
29. Nath, S.; Praharaj, S.; Panigrahi, S.; Basu, S.; Pal, T. Curr Sci 2007, 92, 786.
30. Cliffel, D. E.; Zamborini, F. P.; Gross, S. M.; Murray, R. W. Langmuir 2000, 16, 9699.
31. Alvarez, J.; Liu, J.; Roman, E.; Kaifer, A. E. J Chem Soc Chem Commun 2000, 1151.
32. Narayanan, R.; El-Sayed, M. A. J Phys Chem B 2004, 108, 8572.
33. Li, Y.; Hong, X. M.; Collard, D. M.; El-Sayed, M. A. Org Lett 2000, 2, 2385.
34. Vincent, T.; Guibal, E. Langmuir 2003, 19, 8475.
35. Tong, J.; Li, Z.; Xia, C. J Mol Catal A 2005, 231, 197.
36. Sun, Y.; Guo, Y.; Lu, Q.; Meng, X.; Xiaohua, W.; Guo, Y.; Wang, Y.; Liu, X.; Zhang, Z. Catal Lett 2005, 100, 213.
37. Mucalo, M. R.; Bullen, C. R.; Manley-Harris, M. J Mater Sci 2002, 37, 493.
38. Kumar, A.; Vemula, P. K.; Ajayan, P. M.; John, G. Nat Mater 2008, 7, 236.
39. Mallikarjuna, N. N.; Varma R. S. Green Chem 2008, 10, 859.
40. Lang, X.; Wu, X. C.; Zhu, J. J. Nanotechnology 2008, 19, 859.
41. Dhar, S.; Reddy, E. M.; Shiras, A.; Pokharkar, V.; Prasad, B. L. V. Chem Eur J. 2008, 14,10244.
42. Bandyopadhyaya, R.; Nativ-Roth, E.; Regev, O.; Yerushalmi Rozen, R. Nano Lett 2002, 2, 25.
43. Kattumuri, V.; Katti, K.; Bhaskaran, S.; Boote, E. J.; Casteel, S. W.; Fent, G. M.; Robertson, D. J.; Chandrasekhar, M.; Kannan, R.; Katti, K. V. Small 2007, 3, 333.
44. Velikov, K. P.; Zegers, G. E.; van Blaaderen, A. Langmuir 2003, 19, 1384.
45. Williams, D. N.; Gold, K. A.; Holoman, T. R. P.; Ehrman, S. H.; Wilson, O. C. J. Nanopart Res 2006, 8, 749.
46. Zhang, H. Y.; Shan, G. B.; Liu, H. Z.; Xing, J. M. Surf Coat Technol 2007, 201, 6917.
47. Park, C.; Lim, K. H.; Kwon, D.; Yoon, T. H. Bull Korean Chem Soc 2008, 29, 1277.
48. Murali Mohan, Y.; Mohana Raju, K.; Sambasivudu, K.; Singh, S.; Sreedhar, B. J Appl Polym Sci 2007, 106, 3375.
49. Inorganic Colloid Chemistry; Weiser, H. B., Ed.; Wiley: New York, 1933–1938.3 vols., p 1–1938.
50. Luo, C.; Zhang, Y.; Zeng, X.; Zeng, Y.; Wang, Y. J Colloid Interface Sci 2005, 288, 444.
51. Washio, I.; Xiong, Y.; Yin, Y.; Xia, Y. Adv Mater 2006, 18, 1745.
52. Hoppe, C. E.; Lazzari, M.; Pardinas-Blanco, I.; Lopez-Quintela, M. A. Langmuir 2006, 22, 7027.
53. Hussain, I.; Brust, M.; Papworth, A. J.; Cooper, A. I. Langmuir 2003, 19, 4831.
54. Ershov, B. G.; Henglein, A. J Phys Chem B 1998, 102, 10663.
55. Shiraishi, Y.; Toshima, N. Colloids Surf A 2000, 69, 59.
56. Tabuani, D.; Monticelli, O.; Chincarini, A.; Bianchini, C.; Vizza, F.; Moneti, S.; Usso, S. Macromolecules 2003, 36, 4294.
57. Samba Sivudu, K.; Mallikarjuna Reddy, N.; Nagendra Prasad, M.; Mohana Raju, K.; Murali Mohan, Y.; Yadav, J. S.; Sabitha, G.; Shailaja D. J Mol Catal A 2008, 295, 10.
58. NIST X-Ray Photoelectron Spectroscopy Database NIST Standard Reference Database 20, Version 3.4. June 06, 2000 http://srdata.nist.gov/xps/.